Publications of the Astronomical Society of the Pacific, 133:044002 (15pp), 2021 April https://doi.org/10.1088/1538-3873/abd417

Low-redshift Type Ia Supernova from the LSQ/LCO Collaboration

C. Baltay[1], L. Grossman[1], R. Howard[1], D. Rabinowitz[1], I. Arcavi[2,3,4], N. Barbour[1,11], J. Burke[2,5], C. Contreras[6], B. Dilday[7], M. Graham[8], D. Hiramatsu[2,5], G. Hossenzadeh[9], D. A. Howell[2,5], C. McCully[2], R. McKinnon[1,12], K. Ment[1,13], R. Montesi[1], C. Pellegrino[2,5], and S. Valenti[10]
[1] Department of Physics, Yale University, USA; charles.baltay@yale.edu
[2] Las Cumbres Observatory (LCO), USA
[3] School of Physics and Astronomy, Tel Aviv University, Israel
[4] CIFAR Azrieli Global Scholars Program, Toronto, Canada
[5] Department of Physics, UC Santa Barbara, USA
[6] Las Campanas Observatory, Chile
[7] Department of Physics and Astronomy, Rutgers University, USA
[8] Physics Department, University of Washington, USA
[9] Center for Astrophysics, Harvard & Smithsonian, USA
[10] Department of Physics, UC Davis, USA
Received 2020 October 1; accepted 2020 December 16; published 2021 March 26

Abstract

This paper is the data release of a new sample of 140 type Ia supernovae (SNe Ia) from the LaSilla-QUEST/Las Cumbres Observatory (LCO) collaboration. The discovery of the supernovae came from the LaSilla-QUEST variability survey, the ASASSN survey, as well as smaller low redshift supernova surveys. All of the supernovae in this sample were spectroscopically identified as SNe Ia using spectra from the PESSTO survey using the 3.5 m NTT telescope at LaSilla and spectra from the LCO 2 m Faulkes telescopes. The light-curves were obtained from a rapid cadence photometric follow up of the supernovae with the 9 LCO 1 m telescopes located at various observatories around the globe. Reference images of the host galaxies were taken approximately a year after the supernova have faded to allow precise galaxy background subtraction from the supernova magnitudes. The supernovae in this sample were discovered over a seven year period from 2012 October to 2019 June, and the last galaxy reference images were taken before 2020 June.

Unified Astronomy Thesaurus concepts: Type Ia supernovae (1728); Spectroscopy (1558); Supernovae (1668)

Online material: machine-readable tables

1. Introduction

A collaboration of the LaSilla/QUEST Southern Hemisphere Variability Survey (LSQ) (Baltay et al. 2013) using the 10 square degree QUEST camera on the ESO I meter Schmidt telescope and the Key Supernova Project (Howell et al. 2015) of the Las Cumbres Observatory (LCO) using nine 1 m telescopes for imaging (see Table 1) and two 2 m telescopes for spectroscopy have carried out a low redshift Type Ia supernova (SN Ia) survey. This paper presents the resulting 140 supernova light-curves. The supernova were discovered by the LSQ survey, the ASASSN survey (Holoien et al. 2017), and a number of surveys with smaller telescopes. All of the supernova in this sample were spectroscopically identified as SN Ia with a spectroscopic redshift measurement. The spectra were taken by the PESSTO collaboration (Smartt et al. 2015) using the EFOSCII spectrometer on the NTT telescope at LaSilla and the two 2 m LCO Faulkes telescopes (Brown et al. 2013), the Faulkes North at Haleakala, Maui, and the Faulkes South at Siding Springs, Australia.

A large sample of low redshift supernovae will be needed to help understand the nature of the SNe Ia and to anchor the Hubble diagram of high redshift supernova samples. For this reason a number of surveys have been carried out to collect samples of low-redshift supernovae. The currently available samples of published low-redshift Type Ia light curves have been collected recently (Rest et al. 2014; Scolnic et al. 2018). They find a total of 497 supernovae which is reduced to a sample of 222 when the required quality cuts are made. A loose collaboration of a number of groups have undertaken the task of collecting a larger number of low-redshift supernovae: the Supernova Factory (Aldering et al. 2002), the Carnegie Supernova Project CSPII (Phillips et al. 2019), the Palomar

[11] Present Address: Physics Department University of Maryland.
[12] Present Address: Physics Department MIT.
[13] Present Address: Physics Department Harvard University.

Table 1
LCO 1 m Telescopes

Telescope No	Host Observatory	Location
4	Cerro Tololo	Chile
5	Cerro Tololo	Chile
9	Cerro Tololo	Chile
8	McDonald	Texas, USA
3	Siding Springs	Australia
11	Siding Springs	Australia
10	SAAO Sunderland	South Africa
12	SAAO Sunderland	South Africa
13	SAAO Sunderland	South Africa

Transient Factory (PTF) (Maguire et al. 2014), the La Silla-QUEST Survey (LSQ), the ASAS-SN collaboration, and a number of surveys using smaller than 0.5 m telescopes referred to in Table 2. These various samples, each calibrated in their particular way, will need to be combined, with care taken to calibrate them in a uniform way that is consistent with the calibration of the high redshift samples.

In what follows, Section 2 describes the supernova discovery surveys and spectroscopy, and Section 3 describes the imaging to obtain the light curves. Section 4 describes the data set, and Section 5 describes the data analysis methods. The results and conclusions are given in Sections 6 and 7.

2. Supernova Discoveries and Spectroscopy

The surveys that discovered the supernova in this sample are indicated on Table 2.

2.1. The La Silla-QUEST Southern Hemisphere Variability Survey (LSQ)

The LSQ Variability Survey was initiated with the purpose of discovering low-redshift supernovae (Baltay et al. 2013). The survey used the 1.0 m ESO Schmidt telescope at the La Silla Observatory in Chile. For this survey it was equipped with the 10 square degree QUEST camera (Baltay et al. 2007). The camera consisted of 112 Sarnoff CCD's with 13 μm pixels that corresponded to $0\farcs87$ on the sky. The survey operated typically with 60 s exposures, was sensitive to SNe Ia up to a redshift of 0.12, and covered the sky between decl. of $+20^\circ$ and -40° except for the region of the Milky Way. The survey was an untargeted search for transients in that it searched large areas of the sky with no bias with respect to the presence or absence or the properties of galaxies in the search areas. The supernova search operated from 2011 to 2016, with 448 spectroscopically confirmed supernova: 317 Type Ia, 35 Type Ibc, and 96 type II. All spectroscopically confirmed supernova were announced within 24 hr via ATELs so they could be followed up by any of the collaborating groups as desired. The majority of the supernovas followed by the SNf and the CSPII groups were LSQ discoveries.

2.2. All Sky Automated Survey for SuperNovae (ASAS-SN)

The ASAS-SN survey (Holoien et al. 2017) uses 24 telescopes each consisting of four 14 cm cameras with $8''$ pixels distributed all over the globe so that their supernova search is going on at any time in many locations. The telescopes have a single V filter and are sensitive to a magnitude of $m_V < 17$. It is a low-redshift bright supernova search with redshifts typically less than $z = 0.04$. With a rapid search cadence of 2–3 days the survey finds many early supernovas. The search is untargeted with respect to the presence of galaxies. The survey started in 2013 April and is still operating. All supernova discoveries are announced in ATELs so they can be followed up by a variety of collaborations.

2.3. Surveys with Smaller Telescopes

There are a number of smaller supernova surveys with telescopes typically 0.5 m or less. These surveys, some by professional groups and some by amateur astronomers, are sensitive to supernovas typically with redshifts below 0.03. The discoveries by these groups are announced rapidly after discovery and many of them were followed with imaging for light curves by the LCO 1 m telescopes. The references for these surveys for supernovae that are in the present sample are given in Table 2 below.

2.4. Spectroscopy

All of the supernovae in this sample were identified as SN Ia and their redshift has been measured by high quality spectra. There were two sources of spectroscopy used for this sample. One was the PESSTO Collaboration using the 3.5 m NTT telescope with the EFOSCII spectrometer at the La Silla observatory in Chile (Smartt et al. 2015). The second source was the two 2 m Faulkes telescopes (the Faulkes North at Haleakala, Maui, and the Faulkes South at Siding Springs, Australia) with the identical FLOYDS spectrometers by the LCO observatory (Howell et al. 2015). Some fraction of the sample had spectra taken by both. A sample spectrum taken by PESSTO is shown in Figure 1. All of the spectra used in the analysis of this sample can be found on the WISEREP Supernova Data Base (Yaron & Gal-Yam 2012). The reduced and calibrated PESSTO spectra (and associated data products) are also available through ESO's Science Archive Facility (see www.pessto.org for details on how to access these).

3. Imaging for Light Curves

All of the imaging to obtain the light curves for the low-redshift sample presented in this paper were obtained by the LCO Supernova Key Project (Howell et al. 2015) with the nine 1 m telescopes of the Las Cumbres Observatory (LCO). A list of these telescopes, their host observatories and locations, is in Table 1.

Table 2
The Final Sample of Low-redshift Supernovae

No	Name	R.A.	Decl.	Redshift	Discovery[a]	Spectroscopy[a]	Discovery Phase	1st Point Phase
1	ASASSN-14jg	23:33:13.90	−60:34:11.5	0.015	ASAS-SN	PESSTO/LCO	−11	7
2	ASASSN-14kd	22:53:24.95	04:47:57.3	0.026	ASAS-SN	PESSTO	−9	1
3	ASASSN-14lp	12:45:09.10	−00:27:32.5	0.005	ASAS-SN	PESSTO/LCO	−15	−13
4	ASASSN-14lw	01:06:49.17	−46:58:60.0	0.015	ASAS-SN	PESSTO	−11	−5
5	ASASSN-14mg	02:53:58.10	−21:38:52.9	0.031	ASAS-SN	PESSTO	12	12
6	ASASSN-15hf	10:29:30.76	−35:15:35.2	0.005	ASAS-SN	PESSTO/LCO	−11	−8
7	ASASSN-15hx	13:43:16.69	−31:33:21.5	0.008	ASAS-SN	PESSTO/LCO	−14	−13
8	ASASSN-15hy	20:10:02.35	−00:44:21.3	0.025	ASAS-SN	PESSTO/LCO	−15	−13
9	ASASSN-15jo	14:06:44.67	−34:27:17.4	0.015	ASAS-SN	LCO	−7	−4
10	ASASSN-15 kg	08:40:12.01	−04:35:31.0	0.014	ASAS-SN	LCO	−10	−8
11	ASASSN-15mc	02:48:59.57	03:10:10.5	0.014	ASAS-SN	LCO	−9	−8
12	ASASSN-15pl	02:30:23.17	−20:41:00.1	0.016	ASAS-SN	LCO	−15	−1
13	ASASSN-15ps	06:14:46.20	−66:13:01.0	0.040	ASAS-SN	LCO	−19	−13
14	ASASSN-15rq	00:08:03.14	−36:33:51.8	0.025	ASAS-SN	PESSTO/LCO	−9	−4
15	ASASSN-15uh	09:30:13.69	69:07:02.5	0.014	ASAS-SN	LCO	−13	−11
16	ASASSN-16ex	17:10:23.92	26:23:47.9	0.032	ASAS-SN	LCO	−13	−10
17	ASASSN-16hp	13:34:38.64	−23:40:53.1	0.009	ASAS-SN	PESSTO/LCO	−17	−5
18	ASASSN-16hw	21:53:27.88	−34:24:20.9	0.014	ASAS-SN	PESSTO/LCO	−11	−2
19	ASASSN-16ke	23:37:56.62	27:16:37.7	0.028	ASAS-SN	LCO	−11	−9
20	AT 2016ayg	07:30:17.40	25:01:56.0	0.045	PTSS	PESSTO	−11	−5
21	CSS140914	01:01:07.04	−10:18:39.9	0.030	CRTS	PESSTO	−12	−3
22	LSQ12fhs	22:52:23.45	−20:36:53.3	0.033	LSQ	PESSTO/LCO	1	17
23	LSQ12fxd	05:22:16.99	−25:35:47.0	0.032	LSQ	PESSTO	−16	−10
24	LSQ12gdj	23:54:43.30	−25:40:34.2	0.030	LSQ	PESSTO	−15	−8
25	LSQ12hzs	04:01:53.17	−26:39:49.7	0.072	LSQ	PESSTO	−8	−3
26	LSQ13aiz	13:15:14.81	−17:57:55.8	0.009	LSQ	LCO	−13	−10
27	LSQ13apt	22:10:34.27	−22:39:47.9	0.031	LSQ	PESSTO	−7	−1
28	LSQ13avx	16:46:01.93	06:27:59.3	0.025	LSQ	PESSTO	−11	5
29	LSQ13beu	00:08:23.11	−20:52:15.2	0.070	LSQ	PESSTO	−13	−1
30	LSQ13bic	22:11:54.31	03:29:39.1	0.070	LSQ	PESSTO	−8	1
31	LSQ13bjq	22:00:48.53	−13:07:17.2	0.070	LSQ	PESSTO	2	5
32	LSQ13bjs	22:09:25.32	−01:38:52.8	0.033	LSQ	PESSTO	−1	1
33	LSQ13bor	03:25:49.06	−19:18:10.6	0.110	LSQ	PESSTO	−7	−5
34	LSQ13bug	21:09:04.07	−26:54:19.9	0.029	LSQ	PESSTO	−6	−10
35	LSQ13bwa	01:18:41.78	−07:26:40.9	0.018	LSQ	PESSTO	−5	−1
36	LSQ13bwl	23:33:55.42	04:31:00.2	0.070	LSQ	PESSTO	4	8
37	LSQ13ccs	01:32:09.46	−23:03:15.1	0.052	LSQ	PESSTO	−4	−2
38	LSQ13cnl	00:14:56.00	−30:33:26.1	0.065	LSQ	PESSTO	−14	−5
39	LSQ13cpk	02:31:03.77	−20:08:49.6	0.033	LSQ	PESSTO	−14	−12
40	LSQ13cto	23:22:40.49	−21:27:19.4	0.120	LSQ	PESSTO	−10	−5
41	LSQ13cwp	04:03:50.66	−02:39:18.0	0.067	LSQ	PESSTO	−7	−4
42	LSQ13deq	04:31:10.22	−26:45:14.4	0.110	LSQ	PESSTO	−12	−8
43	LSQ13der	04:46:39.96	−26:59:15.7	0.060	LSQ	PESSTO	−5	−3
44	LSQ13dny	03:42:16.88	−04:43:18.5	0.014	LSQ	LCO	−17	−16
45	LSQ13ry	10:32:48.00	04:11:51.4	0.030	LSQ	PESSTO	−15	−9
46	LSQ13vy	16:06:55.85	03:00:15.1	0.032	LSQ	LCO	−6	0
47	LSQ14dsu	20:22:00.84	−51:47:46.3	0.020	LSQ	PESSTO	−11	−9
48	LSQ14dtt	21:33:10.25	−18:20:26.2	0.050	LSQ	PESSTO	−33	−5
49	LSQ14eef	21:23:33.46	−08:45:36.7	0.060	LSQ	PESSTO	−32	−5
50	LSQ14fep	03:02:24.99	−58:07:56.5	0.060	LSQ	PESSTO	−12	−9
51	LSQ14few	02:19:59.64	−55:32:50.2	0.060	LSQ	PESSTO	−9	−6
52	LSQ14fms	00:14:59.82	−51:12:39.5	0.070	LSQ	PESSTO	−5	−4
53	LSQ14foj	00:26:34.68	−32:48:33.1	0.046	LSQ	PESSTO	−18	−12
54	LSQ14fom	21:59:49.73	−30:16:15.6	0.060	LSQ	PESSTO	−14	−8
55	LSQ14fvy	05:29:06.07	−35:11:38.3	0.057	LSQ	PESSTO	−12	−6
56	LSQ14fyc	23:47:40.17	−13:58:54.9	0.082	LSQ	PESSTO	−16	−11
57	LSQ14gie	04:08:22.05	−09:54:10.7	0.070	LSQ	PESSTO	−18	−10
58	LSQ15aae	16:30:15.70	05:55:58.7	0.050	LSQ	PESSTO	−6	−5

Table 2
(Continued)

No	Name	R.A.	Decl.	Redshift	Discovery[a]	Spectroscopy[a]	Discovery Phase	1st Point Phase
59	LSQ15agh	10:52:54.78	23:35:43.0	0.060	LSQ	LCO	−18	−8
60	LSQ15bv	10:59:47.28	−16:49:10.6	0.060	LSQ	LCO	−10	−6
61	LSQ16acz	14:20:18.05	−22:11:20.8	0.053	LSQ	LCO	−20	−11
62	LSQ16ha	12:05:25.82	−21:24:02.2	0.032	LSQ	LCO	−11	6
63	PS15sv	16:13:11.74	01:35:31.1	0.038	PS1	PESSTO/LCO	−10	−4
64	PSN J08351668	08:35:16.68	48:19:01.1	0.043	TNTS	LCO/PESSTO	−14	−11
65	PSN J22412689	22:41:26.89	39:17:22.0	0.017	Ref 1	LCO	−13	−4
66	PSN J23374322	23:37:43.21	−47:30:39.3	0.010	MASTER	LCO/PESSTO	−12	−2
67	SN 2012ht	10:53:22.75	16:46:34.9	0.004	Ref 2	LCO/PESSTO	−16	−11
68	SN 2014cd	04:23:47.24	−51:36:03.1	0.020	Ref 3	LCO	−6	−5
69	SN 2014dg	03:48:19.78	70:07:54.5	0.004	Ref 4	LCO	−14	−5
70	SN 2014dl	16:29:46.09	08:38:30.6	0.033	CRTS	LCO/PESSTO	−11	−6
71	SN 2014eg	02:45:09.27	−55:44:16.9	0.018	PESSTO	LCO/PESSTO	−15	−7
72	SN 2014J	09:55:42.14	69:40:26.0	0.001	Ref 5	LCO/PESSTO	−12	−12
73	SN 2015ak	22:15:19.67	−65:32:53.4	0.010	Ref 6	LCO	−15	−15
74	SN 2015F	07:36:15.76	−69:30:23.0	0.004	Ref 7	LCO/PESSTO	−16	−15
75	SN 2015N	21:43:16.89	43:34:47.6	0.019	PS1	LCO	−14	−6
76	SN 2016aqt	13:45:50.75	26:47:47.4	0.050	Ref 8	LCO	−5	1
77	SN 2016asf	06:50:36.73	31:06:44.6	0.021	ASAS-SN	LCO	−12	−7
78	SN 2016bln	13:34:45.49	13:51:14.3	0.024	PTF	PESSTO	−18	−16
79	SN 2016ccp	01:02:39.90	−49:39:25.1	0.030	ATS	LCO	−7	−1
80	SN 2016eii	03:07:53.50	−69:01:47.2	0.036	Gaia	LCO	−14	−7
81	SN 2016eoa	00:21:23.10	22:26:08.3	0.021	Ref 8	LCO	−13	−3
82	SN 2016hvl	06:44:02.16	12:23:47.8	0.013	ATLAS	LCO/PESSTO	−12	6
83	SN 2016iks	23:07:21.47	02:54:28.3	0.063	CRTS	LCO/PESSTO	−20	−18
84	SN 2017awz	11:07:35.49	22:51:04.4	0.022	ATLAS	LCO/PESSTO	−12	−9
85	SN 2017azw	04:22:49.71	−82:04:09.6	0.020	ASAS-SN	LCO/PESSTO	−12	−3
86	SN 2017cbv	14:32:34.38	−44:08:03.1	0.004	DLT40	LCO/PESSTO	−18	−18
87	SN 2017cfd	08:40:49.14	73:29:15.1	0.012	PS1	LCO	−16	−11
88	SN 2017ckq	10:44:25.39	−32:12:32.8	0.010	ATLAS	LCO	−16	−7
89	SN 2017drh	17:32:26.06	07:03:47.5	0.006	DLT40	LCO	−14	−7
90	SN 2017ejb	12:48:36.01	−41:19:33.5	0.010	DLT40	LCO/PESSTO	−8	−1
91	SN 2017erp	15:09:14.81	−11:20:03.2	0.006	Ref 4	LCO	−17	−16
92	SN 2017exo	18:31:41.90	16:39:07.3	0.016	ASAS-SN	LCO	−8	0
93	SN 2017fbp	03:17:27.86	−00:05:11.3	0.023	ASAS-SN	LCO	−11	−10
94	SN 2017fgc	01:20:14.45	03:24:10.1	0.008	DLT40	LCO	−15	−13
95	SN 2017fzw	06:21:34.77	−27:12:53.5	0.005	DLT40	LCO/PESSTO	−13	−9
96	SN 2017gah	22:02:42.43	−32:47:33.4	0.009	ATLAS	LCO/PESSTO	−8	−2
97	SN 2017hng	04:21:40.59	−03:32:26.4	0.030	PTSS	LCO	−16	−10
98	SN 2017hpa	04:39:50.75	07:03:54.9	0.016	Ref 8	LCO	−15	−13
99	SN 2017isj	11:10:44.56	04:50:51.1	0.019	ASAS-SN	LCO	−4	−2
100	SN 2017ixg	23:20:30.57	24:46:39.4	0.028	TNTS	LCO	−13	−10
101	SN 2017yh	17:52:06.25	21:33:58.3	0.020	ASAS-SN	LCO	−8	−4
102	SN 2018aaz	10:13:48.24	38:45:47.4	0.023	Ref 4	LCO	−8	−6
103	SN 2018adf	13:18:42.77	−00:45:33.0	0.113	PS1	LCO	−8	−5
104	SN 2018agk	13:10:36.39	−04:29:08.7	0.026	KEGS	LCO	−17	−11
105	SN 2018aoz	11:51:01.79	−28:44:38.4	0.006	DLT40	PESSTO	−12	−12
106	SN 2018bgz	14:49:38.29	25:22:12.7	0.034	CRTS	PESSTO	−16	−9
107	SN 2018bie	12:35:44.32	−00:13:16.0	0.022	ATLAS	LCO/PESSTO	−17	−14
108	SN 2018bta	16:57:58.75	−62:43:53.7	0.020	Ref 3	LCO/PESSTO	−11	−5
109	SN 2018cni	15:01:22.83	−10:10:49.9	0.032	PTSS	LCO/PESSTO	5	10
110	SN 2018fhw	04:18:06.16	−63:36:56.7	0.017	ASAS-SN	LCO	−6	−4
111	SN 2018gv	08:05:34.61	−11:26:16.3	0.005	Ref 4	LCO/PESSTO	−17	−16
112	SN 2018hgc	00:42:04.56	−02:37:40.8	0.052	CRTS	LCO/PESSTO	−15	−8
113	SN 2018hhn	22:52:32.06	11:40:26.7	0.029	Ref 1	LCO/PESSTO	−12	−9
114	SN 2018hkx	04:00:53.81	−66:40:30.6	0.025	ASAS-SN	LCO	−13	−11
115	SN 2018hpu	03:18:21.22	−41:36:34.9	0.067	ASAS-SN	LCO	−4	8

Table 2
(Continued)

No	Name	R.A.	Decl.	Redshift	Discovery[a]	Spectroscopy[a]	Discovery Phase	1st Point Phase
116	SN 2018hss	04:13:00.21	−53:59:33.8	0.043	ASAS-SN	LCO	−6	2
117	SN 2018hsz	03:56:20.64	−54:00:38.8	0.062	ASAS-SN	LCO	0	8
118	SN 2018ilu	23:33:20.98	04:48:34.7	0.018	ATLAS	LCO/PESSTO	−16	−13
119	SN 2018ioa	04:20:32.12	−38:57:35.9	0.041	ASAS-SN	LCO	−7	−6
120	SN 2018isq	03:16:50.60	80:47:04.5	0.008	Ref 8	LCO	−7	−6
121	SN 2018jhf	00:35:54.72	−75:38:15.7	0.058	OGLE	LCO/PESSTO	−12	−5
122	SN 2018jky	03:26:01.93	−17:33:48.0	0.015	ASAS-SN	LCO/PESSTO	−12	−11
123	SN 2018jwi	06:18:39.28	−54:28:14.8	0.015	ASAS-SN	PESSTO	−11	7
124	SN 2018las	10:59:52.23	19:47:41.8	0.027	ZTF	LCO	−13	0
125	SN 2018oh	09:06:39.59	19:20:17.5	0.011	ASAS-SN	LCO/PESSTO	−11	−8
126	SN 2018pc	09:28:55.17	49:14:17.3	0.009	TNTS	LCO	−12	−8
127	SN 2018ph	08:11:02.30	05:05:13.9	0.030	Ref 8	PESSTO	−7	3
128	SN 2018xx	12:53:48.26	−39:41:49.6	0.010	DLT40	LCO	−14	−14
129	SN 2018yu	05:22:32.36	−11:29:13.8	0.008	DLT40	LCO/PESSTO	−17	−16
130	SN 2019bka	11:44:25.76	−11:29:13.8	0.018	ASAS-SN	LCO/PESSTO	−11	−4
131	SN 2019cth	14:45:47.50	50:23:49.0	0.013	Ref 8	LCO	−20	−16
132	SN 2019cxu	13:05:30.09	−08:45:52.7	0.043	ZTF	LCO	−3	−1
133	SN 2019cxx	11:17:48.22	13:43:42.0	0.025	Ref 9	LCO/PESSTO	−15	−9
134	SN 2019dfa	09:58:59.81	17:49:07.7	0.026	ATLAS	LCO	−14	−13
135	SN 2019dks	11:44:05.60	−04:40:25.2	0.057	ZTF	LCO	−16	−12
136	SN 2019eim	23:49:42.93	−69:42:02.3	0.039	ASAS-SN	LCO/PESSTO	−3	1
137	SN 2019gbx	12:50:02.80	−14:46:00.2	0.013	ATLAS	LCO/PESSTO	−15	−15
138	SN 2019np	10:29:21.96	29:30:38.4	0.005	Ref 4	LCO	−18	−16
139	SN 2019so	12:42:36.43	−40:44:47.0	0.015	ATLAS	LCO/PESSTO	−11	−8
140	UGC766_PSN	01:13:30.63	49:36:34.9	0.018	MASTER	LCO	3	6

Notes. ASAS-SN: All Sky Automated Survey for SuperNovae, Holoien et al. (2017). ATLAS: Asteroid Terrestrial-imaging Last Alert System, Tonry et al. (2018). ATS: Antarctic Transient Survey, Quiang et al. (2018). CRTS: Catalina Realtime Transient Survey, Drake et al. (2009). DLT40: Distance Less Than 40 Mpc Survey, Hosseinzadeh et al. (2017). Gaia :Gaia ESA Space Survey, Brown et al. (2018). KEGS: Kepler Extra-Galactic Survey, Olling et al. (2015). LCO: Las Cumbres Observatory 2 m Faulkes Telescopes, Brown et al. (2013). LSQ: La Silla-QUEST Variability Survey, Baltay et al. (2013). MASTER: Master Global Robotic Net, Lipumov et al. (2010). OGLE: Optical Gravitational Lensing Experiment, Udalsky et al. (1997). PESSTO: Public ESO Spectroscopic Survey of Transient Objects, Smartt et al. (2015). PS1: Pan STARRS 1 Survey, Chambers et al. (2016). PTF: Palomar Transient Factory, Law et al. (2008). PTSS: Purple Mountain Obs-Tsinghua Supernova Survey, Zhang et al. (2020). TNTS: THU-NOAC Transient Survey, Zhang et al. (2014). ZTF: Zwicky Transient Facility, Dekany et al. (2020). Ref 1: J. Grzegorzek, TNS AstronomicalTransient Telegram 23507. Ref 2: K. Nishiyama and F. Kabashima, CBET 3349. Ref 3: S. Parker, CBET 3941. Ref 4: K. Itagaki, CBET 3978. Ref 5: S. J. Fossey, CBET 3792. Ref 6: P. Marples, CBET 4148. Ref 7: B. Monard, CBET 4081. Ref 8: T. Pucket, TNS AstronomicalTransient Telegram 1219. Ref 9: N. Tominaga et al., TNS Astronomical Transient Telegram 32187.

[a] References for the supernova discovery and the source of the spectroscopy are given at the end of the paper. The last two columns of the table are the phase at discovery and the phase of the first point on the lightcurves in units of days past *B* band maximum brightness. LCO stands for Las Cumbres Observatory.

These nine telescopes are identical in design and implementation (Brown et al. 2013). They each have a 1.0 m clear aperture with Ritchey–Chrétien optics, equatorial mounts, and Cassegrain foci at $f/8$. They were put into service in 2012–2013. They are operated as a global network in an automatic fashion with centralized computer-controlled scheduling. There are two models of cameras used. The SBIG (Santa Barbara Instrument Group) camera has $4K \times 4K$ pixel CCDs (Kodak KAF16830) with $0\farcs23$ pixels with a field of view of $26' \times 26'$. The Sinistro cameras have $4K \times 4K$ CCDs Fairchild Imaging FI486) with $0\farcs39$ pixels and a $27' \times 27'$ field of view. All of the telescopes had SBIG cameras initially, but were gradually replaced by the Sinistro cameras, and today they all have the Sinistro cameras. All of the cameras use Bessel *B* and *V* and Gunn *g*, *r*, *i* filters. The filter sets for all nine cameras are identical, simplifying the determination of the color terms.

The imaging with the LCO 1 m telescopes proceeded in the following way. Supernova discoveries were posted on the LSQ or other discovery group webpage typically later in the day after discovery. PESSTO or other spectroscopy telescopes then scheduled taking a spectrum as soon as practical, typically one or two nights after the discovery was posted. The spectra were identified as supernovae and classified by type using the Superfit, SNID or GELATO supernova classification codes. The spectroscopically confirmed supernovae were announced by ATELs within 24 hr and also posted on the PESSTO or other spectroscopy group websites. LCO then scheduled spectroscopically confirmed Type Ia for imaging with a two or three day repeat cadence usually in the *B*, *V*, *g*, *r*, and *i*

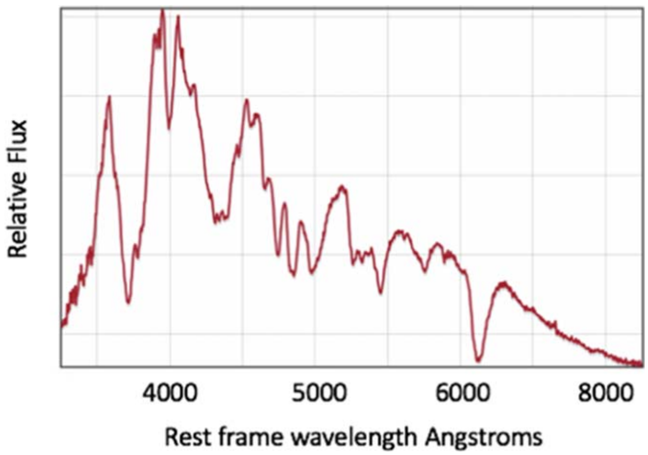

Figure 1. PESSTO spectrum of supernova LSQ12fxd taken on the NTT telescope at La Silla Observatory.

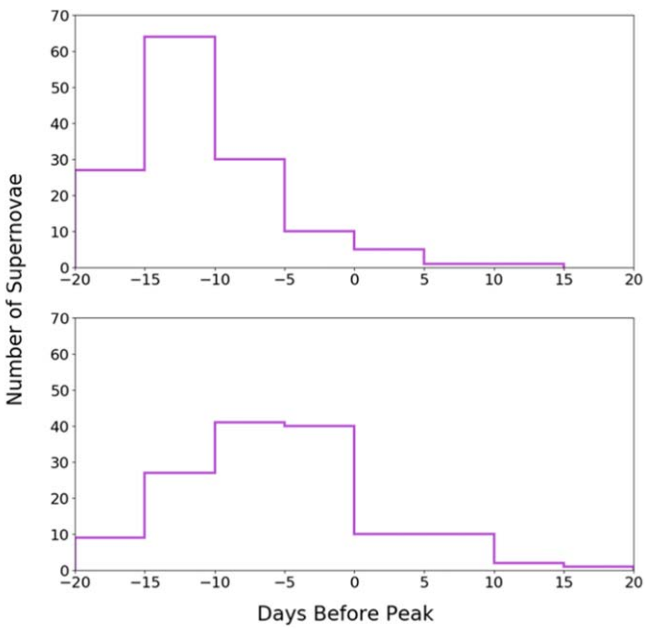

Figure 2. Distribution of the phases of the supernovae in this sample at discovery (upper histogram) and at the first point on the light curve (lower histogram), in days after *B* band peak.

filters. Thus the first points on the light curves were delayed typically by three to five days from the time of discovery. The phases of the supernovae relative to the *B* band maxima at both discovery and at first point on the light curve are shown in Figure 2. The magnitudes of the images along the light curve were carefully monitored. If the points were inconsistent with the light curve for a supernova the imaging was discontinued; otherwise the imaging was continued for typically six weeks after peak *B* band brightness. Approximately a year after peak brightness when the supernova has faded away a reference image was taken at the location of the supernova to be used to

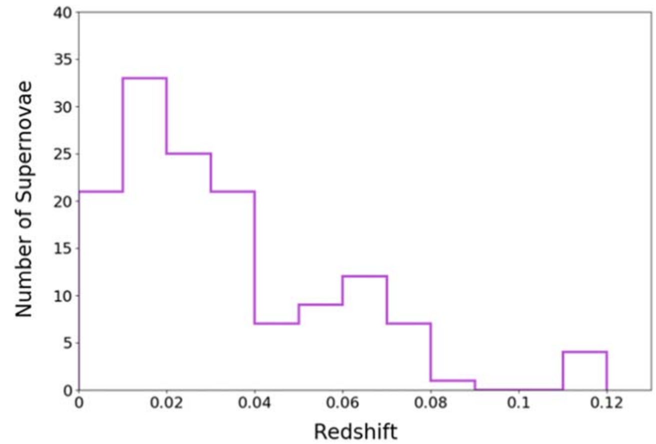

Figure 3. Redshift distribution of the final sample.

subtract the galaxy background light from the images along the light curves.

4. The Data Set

LCO started the supernova imaging campaign with the 1 m telescopes in 2012. Spectroscopically identified SNe Ia that were followed with imaging were entered on the LCO Supernova Exchange database . There was a total of 235 Type Ia's with any images taken starting between 2012 and mid 2019. Of these, 190 had images at more than 6 epochs. These supernovae formed the input sample for the analysis presented in this paper. The galaxy reference images for the supernovae were taken by the 1 m telescopes up to early 2020. After processing this sample through the analysis described in the next section, including the galaxy background subtraction, all of these supernovae were processed by the SALT2.4 analysis program (Guy et al. 2007, 2010; Betoule et al. 2014). A final sample of 140 supernovae had obtained light curves in SALT2.4 in at least three filters with 6 epochs each that were consistent with SNe Ia near or before peak brightness. This final sample is summarized in Table 2 below. The distributions in the phases of the supernovae in this sample at discovery and at the first point on the light curve are given in Figure 2 in days after *B* band maximum. The distribution of this final sample in redshift is shown in Figure 3. The ASASSN supernovae have a lower redshift distribution while the LSQ supernovae are at higher redshifts.

5. Data Analysis

The light curve data for the sample of 190 supernovae in our sample were reduced using a version of the software kindly made available to us by the Carnegie Supernova Project (CSP) as described in Hamuy et al. (2006) and Contreras et al. (2010). These programs were modified at Yale to be suitable for data from the LCO 1 m telescopes, see also Walker et al. (2015).

5.1. Preprocessing and Calculating Instrumental Magnitudes

As the first step, images are bias-subtracted and flat-fielded, after which an astrometric solution is applied. Exposure time variation corrections are also applied. Instrumental magnitudes are then measured for the supernova images as well as a number of selected field stars (local sequence stars) on the same exposure as the supernova and common to all the images for a given target. These were obtained using the SExtractor program (Bertin & Arnouts 1996) with aperture photometry of size comparable to the FWHM of the images.

5.2. Galaxy Background Light Subtraction

Before calibrating supernova magnitudes, we remove the host galaxy light by subtracting a host galaxy reference image taken after the supernova has faded to a negligible level (300 days or more after maximum light). These reference images were taken with the LCO 1 m telescopes and were deeper and taken with seeing conditions that matched or exceeded the seeing conditions for the light curve images. In all cases the same physical filters were used as for the supernova light curve exposures. Two algorithms were used to carry out these galaxy subtractions. One was a fast automated procedure using the HOTPANTS image subtraction program (Becker et al. 2004). All supernovae were run through this fast method. The subtracted images were examined to assess how well the subtraction worked. About two thirds of the supernovae were judged to be successfully subtracted by this method. The remaining third were then processed by a slow manually guided subtraction procedure to obtain satisfactory subtractions.

5.3. Calibration of the Supernova Light Curves

These instrumental magnitudes were then corrected and calibrated using field stars from the APASS catalog Data Release 10 (Henden et al. 2012, 2018). APASS has B, V, u, g, r, i, z filters, which are a good match to the B, V, g, r, i filters used by the LCO telescopes. The magnitudes in the APASS catalog were calibrated using Landolt standard stars (Landolt 2009) for the B and V filters, and the Sloane standard stars (Smith et al. 2002) for the u, g, r, i, z filters. The Landolt standards used the Vega standard system and the Sloane standards used the BD17 standard system. Thus the magnitudes of the supernova presented in this paper were ultimately based on the Vega system for the B and V filters and the BD17 system for the g, r, i filters. The magnitudes of the supernovae in the various filters at the various observation times are given electronically in Table A1 in the Appendix. At this point we had a choice of what filter system to calibrate the light curves to. We chose the natural system of the LCO 1 m telescopes (they all used identical filter sets). These light curves were processed by SALT2.4 later which has the option to use the LCO natural system. The filter transmission as a function of wavelength are a long table and are available electronically as Table A2 as mentioned in Appendix. The quantum efficiencies of the SBIG and the Sinistro cameras are also given electronically as Table A3 discussed in Appendix. The magnitudes in the LCO natural system of the standard stars were B and V of 0.03 for Vega, and for BD17 $g = 9.67$, $r = 9.35$ and $i = 9.25$ (to within ±0.01 for the nine telescopes since they had the identical filters). To calibrate to the LCO natural system we used the color terms given in Table B1 of Valenti et al. (2016) to convert the APASS magnitudes to the LCO natural system using the equations:

$$
\begin{aligned}
B_{\rm nat} &= B_{\rm apass} + C_B(B - V)\\
V_{\rm nat} &= V_{\rm apass} + C_V(B - V)\\
g_{\rm nat} &= g_{\rm apass} + C_g(g - r)\\
r_{\rm nat} &= r_{\rm apass} + C_r(r - i)\\
i_{\rm nat} &= i_{\rm apass} + C_i(r - i)
\end{aligned}
$$

where $B_{\rm apass}$ are the APASS magnitudes, $B_{\rm nat}$ are magnitudes in the LCO natural system, and the C_B are the appropriate color terms (similar for the other filters). These color terms (LCO relative to APASS) have been previously measured and are given in Table B1 of Valenti et al. (2016). They are summarized in Table 3 below for completeness along with the extinction coefficients of the various LCO sites.

The instrumental magnitudes of the field stars that were measured on each exposure of a supernova (typically 20–40 stars) were compared to the their APASS magnitudes (converted to the LCO natural system) for each star to determine their zero-points. The field stars used for this sample of supernovae are given electronically with their APASS magnitudes in Table A4, and with their instrumental magnitudes measured by LCO in Table A5, as discussed in Appendix. The weighted average of the zero-points of all of the field stars was then used to correct the supernova instrumental magnitudes for each point on the light curve.

5.4. Supernova Light Curves

Using the procedure described above, light curves for each of the supernovae in the sample, using aperture photometry, were obtained in each of the filters. All of the light curves in the sample are presented in numerical form in Table 4 (the first twenty lines are in the printed version, and the remainder in various filters are available electronically as Table A1 as discussed in Appendix). The errors on the magnitudes of the points on the light curves have been calculated in the analysis described above and are listed in the table.

5.5. Supernova Template Fitting using SALT2.4

We use the SALT2.4 supernova template fitting program (Guy et al. 2007, 2010; Betoule et al. 2014) to fit the light curves to obtain the best estimate of the rest frame B band peak magnitude for each supernova, the width of its light curve, and its color. SALT2.4 has a large collection of supernova spectra

Table 3
Color Terms and Extinction Coefficients for the LCO 1 m Telescopes

Telescope	Instrument	Filter	Color	Color Term	Extinction Coefficient
3	SBIG	g	$g-r$	0.137 (021)	0.21 (04)
3	SBIG	r	$r-i$	−0.005 (011)	0.10 (04)
3	SBIG	i	$r-i$	0.007 (014)	0.07 (04)
3	SBIG	B	$B-V$	−0.025 (022)	0.20 (06)
3	SBIG	V	$B-V$	0.017 (025)	0.14 (07)
4	Sinistro	g	$g-r$	0.109 (014)	0.14 (03)
4	Sinistro	r	$r-i$	0.027 (013)	0.08 (02)
4	Sinistro	i	$r-i$	0.036 (016)	0.06 (03)
4	Sinistro	B	$B-V$	−0.024 (011)	0.23 (03)
4	Sinistro	V	$B-V$	−0.014 (030)	0.12 (05)
5	SBIG	g	$g-r$	0.120 (018)	0.14 (03)
5	SBIG	r	$r-i$	−0.002 (018)	0.08 (02)
5	SBIG	i	$r-i$	0.019 (022)	0.06 (03)
5	SBIG	B	$B-V$	−0.035 (019)	0.23 (03)
5	SBIG	V	$B-V$	0.000 (036)	0.12 (05)
8	SBIG	g	$g-r$	0.114 (018)	0.15 (07)
8	SBIG	r	$r-i$	−0.004 (017)	0.09 (04)
8	SBIG	i	$r-i$	0.024 (023)	0.07 (04)
8	SBIG	B	$B-V$	−0.039 (022)	0.22 (05)
8	SBIG	V	$B-V$	−0.005 (035)	0.15 (05)
9	Sinistro	g	$g-r$	0.109 (014)	(0.14 03)
9	Sinistro	r	$r-i$	0.027 (013)	0.08 (02)
9	Sinistro	i	$r-i$	0.036 (016)	0.06 (03)
9	Sinistro	B	$B-V$	−0.024 (011)	0.23 (03)
9	Sinistro	V	$B-V$	−0.014 (030)	0.12 (05)
10	SBIG	g	$g-r$	0.112 (016)	0.16 (05)
10	SBIG	r	$r-i$	−0.001 (014)	0.10 (04)
10	SBIG	i	$r-i$	0.013 (022)	0.07 (04)
10	SBIG	B	$B-V$	−0.030 (020)	0.19 (09)
10	SBIG	V	$B-V$	−0.019 (025)	0.14 (06)
11	SBIG	g	$g-r$	0.137 (021)	0.21 (04)
11	SBIG	r	$r-i$	−0.005 (011)	0.10 (04)
11	SBIG	i	$r-i$	0.007 (014)	0.07 (04)
11	SBIG	B	$B-V$	−0.025 (022)	0.20 (06)
11	SBIG	V	$B-V$	0.017 (025)	0.14 (07)
12	SBIG	g	$g-r$	0.112 (016)	0.16 (05)
12	SBIG	r	$r-i$	−0.001 (014)	0.10 (04)
12	SBIG	i	$r-i$	0.013 (022)	0.07 (04)
12	SBIG	B	$B-V$	−0.030 (020)	0.19 (09)
12	SBIG	V	$B-V$	−0.019 (025)	0.14 (06)
13	SBIG	g	$g-r$	0.112 (016)	0.16 (05)
13	SBIG	r	$r-i$	−0.001 (014)	0.10 (04)
13	SBIG	i	$r-i$	0.013 (022)	0.07 (04)
13	SBIG	B	$B-V$	−0.030 (020)	0.19 (09)
13	SBIG	V	$B-V$	−0.019 (025)	0.14 (06)

at various redshifts and phases from previous surveys. It uses these templates to train the program to enable it to fit the light curves in several filter bands and does the K corrections to convert the filter bands to the rest frame of the supernova. In carrying out these fits SALT2.4 puts limits on the range of data it uses. It limits the wavelength to 3000–7000 Å and the phase to −15 to +45 days past B band peak. The reason for this is that the templates used to train SALT2.4 are not reliable outside of these ranges. This means that the i band light curves are not used in the fits. SALT2.4 also has the effective transmission curves of the filters used at several telescopes, including the LCO telescopes, so the light curves in the LCO natural system are acceptable. The inputs to SALT2.4 are the light curves in several filters, the heliocentric redshift, and the Milky Way extinction for each supernova. The Milky Way extinctions are taken from the dust maps (Schlegel et al. 1998) as recalibrated (Schlafly et al. 2011). The distribution in this Milky Way extinction is shown in Figure 4. The output of SALT2.4 is the peak magnitude m_B in the rest frame B band, the stretch factor x_1, the color c, and the time of the peak magnitude of the supernova. The color c equals the excess $B-V$ color over the natural $B-V$ of a typical SNe Ia in the SALT synthetic spectrum. The SALT2.4 results are summarized in Table 5.

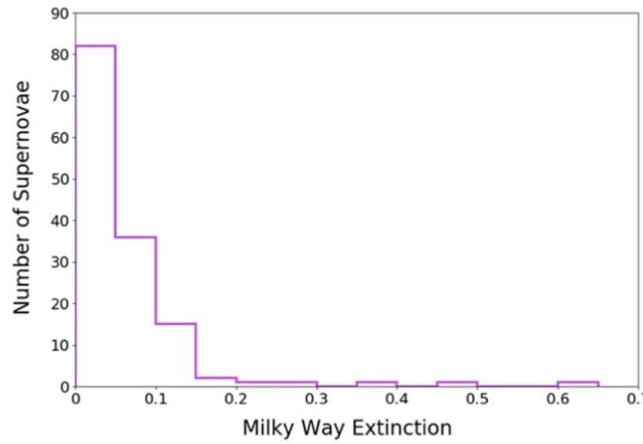

Figure 4. Distribution in the Milky Way extinction for this sample.

Table 4
Supernova Light Curves

Supernova	Filter	JD	m_B	del(m_B)
LSQ13bug	B	2456526.72267	18.089	0.037
LSQ13bug	B	2456526.72631	18.091	0.037
LSQ13bug	B	2456529.52932	17.775	0.029
LSQ13bug	B	2456529.53296	17.751	0.035
LSQ13bug	B	2456530.57598	17.657	0.029
LSQ13bug	B	2456532.60382	17.610	0.027
LSQ13bug	B	2456532.60748	17.616	0.027
LSQ13bug	B	2456534.64398	17.549	0.026
LSQ13bug	B	2456534.64763	17.560	0.026
LSQ13bug	B	2456536.60488	17.620	0.027
LSQ13bug	B	2456536.60853	17.633	0.026
LSQ13bug	B	2456536.63398	17.606	0.027
LSQ13bug	B	2456536.63764	17.615	0.026
LSQ13bug	B	2456540.32889	17.822	0.026
LSQ13bug	B	2456540.33254	17.799	0.027
LSQ13bug	B	2456541.32883	17.872	0.028
LSQ13bug	B	2456541.33248	17.893	0.028
LSQ13bug	B	2456542.33249	17.954	0.034
LSQ13bug	B	2456543.32878	18.074	0.029
LSQ13bug	B	2456543.33244	18.072	0.029

Table 5
SALT Output Parameters for the Final Sample of Low-redshift SNe Ia

No	Name	daymax	z	m_B	mBerr	x_1	x1err	c	cerr
1	ASASSN14jg	2456962.178	0.015	14.930	0.036	1.907	0.124	0.046	0.025
2	ASASSN14kd	2456983.272	0.026	16.322	0.024	2.059	0.360	0.218	0.218
3	ASASSN14lp	2457016.403	0.005	0.005	0.022	0.897	0.042	0.255	0.021
4	ASASSN14lw	2457014.526	0.015	15.651	0.024	1.755	0.231	0.086	0.025
5	ASASSN14mg	2456997.728	0.031	16.241	0.043	0.191	0.075	0.022	0.029
6	ASASSN15hf	2457140.208	0.005	14.029	0.022	2.884	0.067	0.263	0.022
7	ASASSN15hx	2457152.634	0.008	13.221	0.022	0.758	0.052	−0.026	0.021
8	ASASSN15hy	2457152.782	0.025	15.341	0.023	4.079	0.091	0.397	0.023
9	ASASSN15jo	2457169.305	0.015	15.503	0.022	−2.033	0.057	0.171	0.022
10	ASASSN15kg	2457180.348	0.014	15.339	0.024	−1.049	0.098	0.163	0.024
11	ASASSN15mc	2457218.079	0.014	15.344	0.024	1.389	0.123	0.365	0.024
12	ASASSN15pl	2457353.843	0.016	18.428	0.032	5.000	0.041	0.769	0.051
13	ASASSN15ps	2457274.072	0.040	15.007	0.221	−0.834	0.435	−0.829	0.074
14	ASASSN15rq	2457325.348	0.025	15.470	0.037	1.233	0.239	0.061	0.038
15	ASASSN15uh	2457388.420	0.013	14.842	0.035	1.906	0.132	−0.073	0.029
16	ASASSN16ex	2457524.910	0.032	16.816	0.022	3.214	0.105	0.050	0.023
17	ASASSN16hp	2457609.196	0.009	14.085	0.022	−0.411	0.057	0.137	0.022
18	ASASSN16hw	2457604.304	0.014	14.750	0.042	0.943	0.191	0.092	0.030
19	ASASSN16ke	2457650.845	0.028	16.285	0.023	1.950	0.084	−0.005	0.023
20	AT2016ayg	2457468.441	0.045	17.285	0.024	0.086	0.130	−0.072	0.024
21	CSS140914	2456927.001	0.030	16.609	0.024	−0.584	0.077	−0.110	0.024
22	LSQ12fhs	2456204.554	0.033	17.465	0.053	−1.495	0.089	0.376	0.039
23	LSQ12fxd	2456247.521	0.032	16.414	0.031	0.491	0.026	0.073	0.028
24	LSQ12gdj	2456253.376	0.030	15.746	0.033	−1.891	0.090	−0.198	0.029
25	LSQ12hzs	2456298.802	0.072	19.082	0.054	0.204	0.264	0.221	0.045
26	LSQ13aiz	2456437.723	0.009	13.721	0.024	−0.005	0.048	0.052	0.022
27	LSQ13apt	2456449.986	0.031	16.652	0.022	−0.511	0.036	0.004	0.022
28	LSQ13avx	2456464.857	0.025	16.930	0.028	1.966	0.143	0.209	0.025
29	LSQ13beu	2456501.138	0.070	18.109	0.024	0.784	0.168	−0.065	0.024
30	LSQ13bic	456510.277	0.070	18.309	0.022	0.600	0.216	0.064	0.024
31	LSQ13bjq	2456515.596	0.070	18.904	0.029	−0.185	2.230	0.308	0.033
32	LSQ13bjs	2456512.396	0.033	18.159	0.029	−3.071	0.355	0.350	0.026
33	LSQ13bor	2456525.397	0.110	19.454	0.042	2.443	0.462	0.270	0.039
34	LSQ13bug	2456535.447	0.029	17.399	0.021	−0.226	0.050	0.398	0.022
35	LSQ13bwa	2456466.264	0.018	15.002	0.023	1.938	0.157	−0.108	0.023
36	LSQ13bwl	2456520.923	0.070	18.166	0.045	1.615	0.457	−0.094	0.031
37	LSQ13ccs	2456544.257	0.052	17.957	0.022	0.631	0.110	−0.178	0.022
38	LSQ13cnl	2456578.557	0.065	17.884	0.020	2.340	0.099	0.017	0.023
39	LSQ13cpk	2456591.456	0.033	16.469	0.021	0.936	0.047	0.075	0.022
40	LSQ13cto	2456605.175	0.120	19.425	0.031	1.089	0.311	0.158	0.045
41	LSQ13cwp	2456611.838	0.067	19.114	0.042	−2.608	0.376	0.250	0.067
42	LSQ13deq	2456635.020	0.110	19.348	0.026	0.943	0.269	0.040	0.034
43	LSQ13der	2456638.091	0.060	19.925	0.065	5.000	1.033	−4.000	0.030
44	LSQ13dny	2456649.373	0.014	14.828	0.025	−0.462	0.035	0.028	0.021
45	LSQ13ry	2456396.235	0.030	16.573	0.023	−0.337	0.072	−0.004	0.023
46	LSQ13vy	2456395.328	0.032	17.893	0.023	−1.376	0.071	0.178	0.024
47	LSQ14dsu	2456884.053	0.020	15.294	0.022	0.879	0.054	−0.012	0.022
48	LSQ14dtt	2456881.439	0.050	18.869	0.042	−0.562	0.168	0.654	0.035
49	LSQ14eef	2456897.356	0.060	18.358	0.024	1.433	0.414	−0.007	0.027
50	LSQ14fep	2456919.423	0.060	17.794	0.024	0.883	0.133	−0.067	0.025
51	LSQ14few	2456915.981	0.060	17.868	0.027	1.042	0.221	0.044	0.026
52	LSQ14fms	456931.883	0.070	19.114	0.030	−0.621	0.249	0.252	0.030
53	LSQ14foj	2456942.269	0.046	17.413	0.024	0.368	0.110	0.130	0.030
54	LSQ14fom	2456937.956	0.060	17.842	0.022	−0.715	0.116	0.027	0.024
55	LSQ14fvy	2456953.256	0.057	17.989	0.024	−1.418	0.152	−0.029	0.026
56	LSQ14fyc	2456962.952	0.082	18.160	0.024	0.710	0.183	−0.156	0.026
57	LSQ14gie	2457010.945	0.070	18.438	0.027	1.866	0.330	0.048	0.028
58	LSQ15aae	2457117.438	0.050	17.957	0.025	1.097	0.143	0.278	0.026

Table 5
(Continued)

No	Name	daymax	z	m_B	mBerr	x_1	x1err	c	cerr
59	LSQ15agh	2457141.188	0.060	17.926	0.028	1.325	0.181	0.082	0.027
60	LSQ15bv	2457045.035	0.060	18.169	0.046	0.327	0.382	−0.049	0.044
61	LSQ16acz	2457468.077	0.053	17.989	0.049	−1.385	0.847	0.095	0.043
62	LSQ16ha	2457431.796	0.032	16.317	0.044	1.004	0.232	−0.134	0.032
63	PS15sv	2457114.887	0.038	16.528	0.022	0.479	0.100	0.032	0.023
64	PSNJ083516	2457031.480	0.043	17.542	0.030	1.357	0.151	0.074	0.027
65	PSNJ224126	2457266.991	0.017	16.638	0.026	5.000	0.120	0.346	0.031
66	PSNJ233743	2457265.009	0.010	14.249	0.030	−1.717	0.067	−0.091	0.030
67	SN2012ht	2456296.222	0.004	13.200	0.035	−1.095	0.050	0.067	0.030
68	SN2014cd	2456884.789	0.020	16.139	0.022	−0.176	0.052	0.244	0.022
69	SN2014dg	2456926.068	0.004	11.938	0.027	−0.345	0.070	−0.039	0.024
70	SN2014dl	2456936.155	0.033	16.129	0.023	0.821	0.123	0.046	0.022
71	SN2014eg	2456992.780	0.018	15.584	0.032	0.851	0.117	0.267	0.040
72	SN2014J	2456691.372	0.001	11.303	0.027	0.395	0.094	1.044	0.025
73	SN2015ak	2457268.429	0.010	14.727	0.023	0.533	0.055	0.250	0.023
74	SN2015F	2457107.247	0.004	12.786	0.022	−0.988	0.030	0.024	0.021
75	SN2015N	2457222.224	0.019	12.826	0.070	−0.283	0.978	−1.264	0.124
76	SN2016aqt	2457451.915	0.050	17.172	0.026	2.660	0.198	0.091	0.025
77	SN2016asf	2457465.431	0.021	15.547	0.022	0.245	0.067	0.046	0.022
78	SN2016bln	2457500.189	0.024	15.962	0.031	0.928	0.109	−0.019	0.042
79	SN2016ccp	2457521.745	0.030	16.246	0.027	1.279	0.265	−0.066	0.026
80	SN2016eii	2457607.419	0.036	16.694	0.025	0.378	0.096	0.018	0.025
81	SN2016eoa	2457615.921	0.021	15.969	0.023	−1.726	0.069	0.088	0.023
82	SN2016hvl	2457708.766	0.013	14.229	0.027	0.877	0.061	0.112	0.023
83	SN2016iks	2457677.371	0.063	17.241	0.021	5.000	0.002	0.541	0.023
84	SN2017awz	2457813.561	0.022	15.599	0.023	0.331	0.062	0.008	0.024
85	SN2017azw	2457817.658	0.020	14.774	0.022	0.721	0.059	−0.076	0.022
86	SN2017cbv	2457841.157	0.004	11.073	0.021	0.603	0.025	−0.104	0.020
87	SN2017cfd	2457844.690	0.012	14.775	0.027	−0.009	0.057	0.236	0.038
88	SN2017ckq	2457851.697	0.010	14.054	0.022	−0.337	0.034	−0.100	0.021
89	SN2017drh	2457890.802	0.006	16.617	0.023	−1.586	0.048	1.192	0.024
90	SN2017ejb	2457910.127	0.010	15.412	0.024	−2.266	0.048	0.245	0.024
91	SN2017erp	2457935.460	0.006	13.318	0.021	0.200	0.025	0.049	0.021
92	SN2017exo	2457937.345	0.016	15.554	0.022	1.062	0.081	0.165	0.023
93	SN2017fbp	2457946.891	0.023	15.877	0.021	0.387	0.042	0.005	0.021
94	SN2017fgc	2457960.658	0.008	13.593	0.029	0.509	0.036	0.114	0.025
95	SN2017fzw	2457988.338	0.005	14.023	0.022	−2.183	0.037	0.275	0.022
96	SN2017gah	2457983.833	0.009	14.818	0.023	−1.762	0.045	0.331	0.023
97	SN2017hng	2458064.118	0.030	17.163	0.024	1.598	0.083	0.130	0.023
98	SN2017hpa	2458066.723	0.016	14.838	0.022	0.240	0.038	−0.033	0.021
99	SN2017isj	2458093.977	0.019	15.560	0.023	0.174	0.086	0.084	0.024
100	SN2017ixg	2458114.817	0.028	16.063	0.027	1.327	0.121	−0.059	0.024
101	SN2017yh	2457791.670	0.020	15.925	0.023	−1.066	0.058	0.095	0.023
102	SN2018aaz	2458192.372	0.023	17.486	0.031	−5.000	0.208	0.321	0.036
103	SN2018adf	2458193.988	0.113	19.752	0.027	−1.340	0.337	0.163	0.028
104	SN2018agk	2458204.818	0.026	17.019	0.022	0.073	0.047	0.097	0.022
105	SN2018aoz	2458223.046	0.006	12.649	0.022	−1.233	0.027	−0.068	0.021
106	SN2018bgz	2458262.765	0.034	16.689	0.031	0.974	0.051	0.068	0.028
107	SN2018bie	2458266.061	0.022	15.943	0.023	0.917	0.052	0.023	0.022
108	SN2018bta	2458267.080	0.019	15.156	0.022	−0.429	0.048	0.135	0.022
109	SN2018cni	2458277.903	0.032	17.545	0.036	0.318	0.108	0.206	0.026
110	SN2018fhw	2458357.371	0.017	16.575	0.025	−2.331	0.071	0.281	0.025
111	SN2018gv	2458150.961	0.005	12.678	0.021	0.388	0.028	−0.039	0.021
112	SN2018hgc	2458413.284	0.052	17.148	0.020	0 .872	0.047	0.104	0.021
113	SN2018hhn	2458417.649	0.029	16.365	0.022	0.368	0.050	0.059	0.022
114	SN2018hkx	2458420.396	0.025	16.280	0.021	0.659	0.034	0.084	0.021
115	SN2018hpu	2458414.949	0.067	17.694	0.038	−0.061	0.119	−0.213	0.029
116	SN2018hss	2458431.254	0.043	17.648	0.028	−1.590	0.087	−0.021	0.024

Table 5
(Continued)

No	Name	daymax	z	m_B	mBerr	x_1	x1err	c	cerr
117	SN2018hsz	2458424.691	0.062	17.566	0.030	0.048	0.061	−0.026	0.025
118	SN2018ilu	2458450.895	0.018	15.208	0.022	0.777	0.058	−0.042	0.022
119	SN2018ioa	2458448.205	0.041	17.111	0.022	0.420	0.057	0.020	0.022
120	SN2018isq	2458449.895	0.008	15.720	0.026	−4.966	0.512	0.397	0.029
121	SN2018jhf	2458463.128	0.058	17.851	0.025	0.582	0.301	0.224	0.028
122	SN2018jky	2458519.995	0.015	19.491	0.099	5.000	0.058	0.021	0.096
123	SN2018jwi	2458477.404	0.015	14.684	0.025	0.491	0.059	−0.050	0.023
124	SN2018las	2458489.782	0.027	17.612	0.025	−0.474	0.078	0.348	0.024
125	SN2018oh	2458163.645	0.011	14.181	0.022	0.566	0.049	−0.076	0.022
126	SN2018pc	2458165.279	0.009	15.308	0.024	−0.939	0.064	0.281	0.024
127	SN2018ph	2458161.986	0.030	16.416	0.028	−1.954	0.055	−0.076	0.025
128	SN2018xx	2458184.785	0.010	14.150	0.022	−1.454	0.031	−0.017	0.021
129	SN2018yu	2458195.620	0.008	13.529	0.022	0.175	0.031	−0.045	0.021
130	SN2019bka	2458555.930	0.018	15.806	0.022	−0.862	0.053	0.026	0.023
131	SN2019cth	2458596.319	0.013	15.335	0.023	1.433	0.073	0.116	0.022
132	SN2019cxu	2458584.592	0.043	18.684	0.024	−0.476	0.147	0.181	0.025
133	SN2019cxx	2458594.175	0.025	16.232	0.025	0.230	0.077	0.031	0.025
134	SN2019dfa	2458597.977	0.026	16.584	0.023	−0.092	0.062	0.111	0.023
135	SN2019dks	2458599.694	0.057	17.440	0.021	0.974	0.057	−0.079	0.023
136	SN2019eim	2458607.834	0.039	17.419	0.032	−1.429	0.185	0.000	0.028
137	SN2019gbx	2458647.822	0.013	14.684	0.022	−1.515	0.034	−0.064	0.022
138	SN2019np	2458510.926	0.005	13.299	0.023	0.166	0.048	−0.041	0.022
139	SN2019so	2458507.794	0.015	16.614	0.022	−3.255	0.071	0.215	0.023
140	UGC766	2456963.471	0.018	15.499	0.057	−0.112	0.089	0.058	0.028

Several typical light curves with the SALT2.4 fits are shown in Figure 5 (LSQ13dny and LSQ13bug). On the whole the light curves are well sampled and well fitted by the SALT2.4 templates (outlier points were ignored in these fits).

6. Results and Discussion

The values of the SALT output parameters for this sample are summarized in Table 5. The distribution in the stretch parameter x_1 from SALT2.4 is given in Figure 6 and the distribution in the color parameter c is given in Figure 7. These distributions are similar to those obtained in other samples of SNe Ia. The distribution in m_B, the peak B band magnitude in the supernova rest frame given by SALT is shown in Figure 8.

Looking at Figures 6 and 7 we see that there are a few supernovae in the tails of these distributions: beyond $c = 0.4$ in color and beyond $x_1 = 3$ in the stretch parameter. There are also a few supernovae in the tail of the Milky Way extinction distribution, Figure 4. We point this out but do not remove these supernovae from the sample. We do not make any fits for cosmological parameters in this paper. This sample of supernovae is presented here with the presumption that the sample will be used in compilations of low-redshift supernovae to be used in combination with high-redshift samples to determine cosmological parameters. Care will have to be taken at that time to calibrate all of the low and high redshift samples in a uniformly consistent fashion. In those compilations selection criteria can be imposed as appropriate for that particular analysis.

6.1. Error Analysis

It is important to keep track of where the errors on the magnitude of these supernovae come from. As an illustration, Table 6 shows how the errors accumulate for one particular observation of a typical supernova.

Exposure times of 300 s were typical but often longer exposures were used for fainter supernova or for supernovae far from peak magnitude. The instrumental magnitudes were obtained from SExtractor using the formula with an arbitrary additive constant of 25.0:

$$m_{\rm inst} = -2.5 \log({\rm flux}) + 25.0.$$

The galaxy background subtracted photometry had a statistical error that was the error of the instrumental magnitudes of the supernovae combined in quadrature with the error on the galaxy reference image. We estimated a 2% systematic error on the subtraction procedure that was added in quadrature to the statistical error. In this particular case 18 field stars, with a wide variety of colors, were used in the calibration process. The errors on the APASS magnitudes of these field stars varied between 0.05 and 0.15 mag, depending on magnitude. Thus the error on the weighted

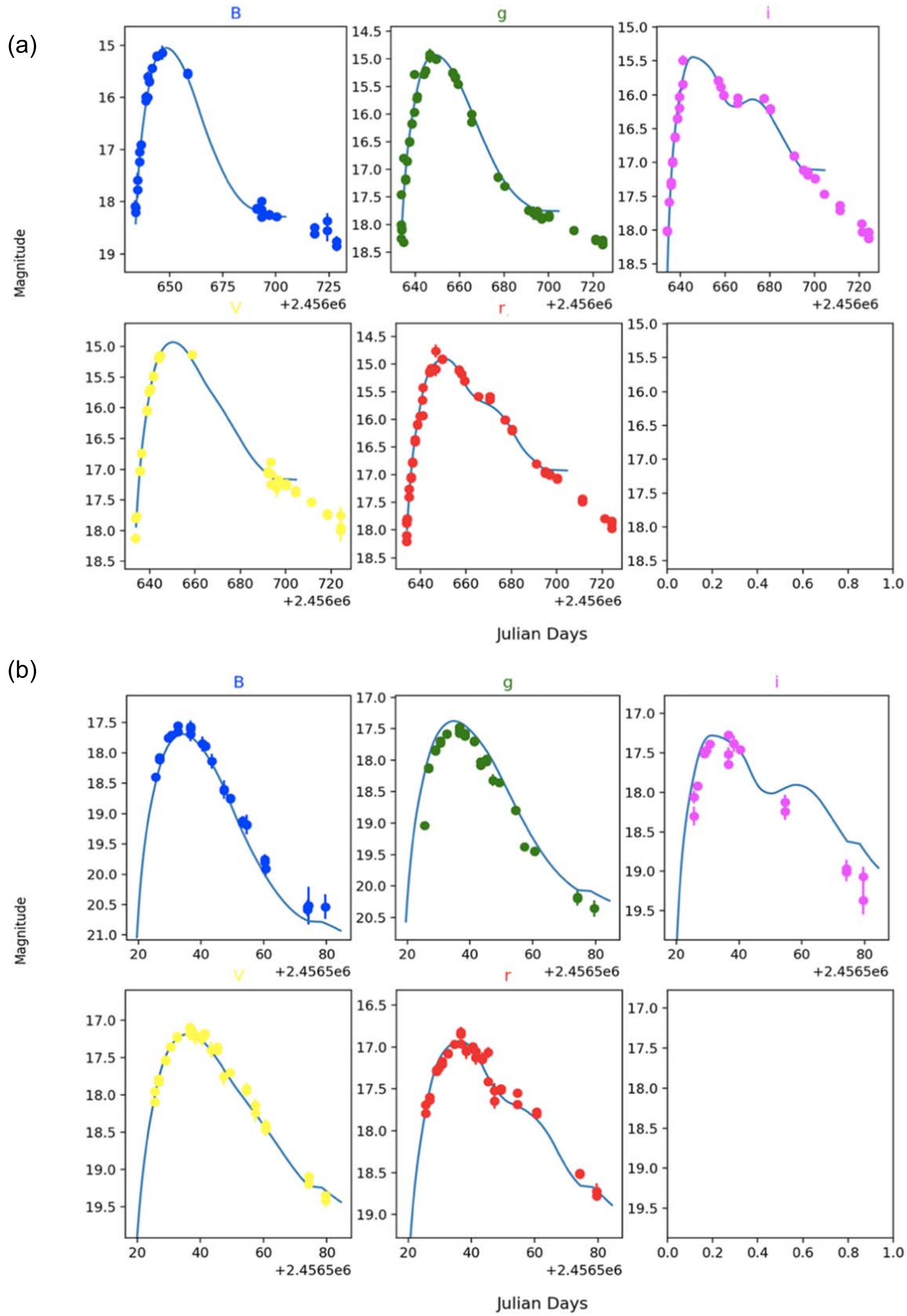

Figure 5. (a) Light curves for Supernova LSQ13dny. The curves are the SALT fits. (b) Light curves for Supernova LSQ13bug. The curves are the SALT fits.

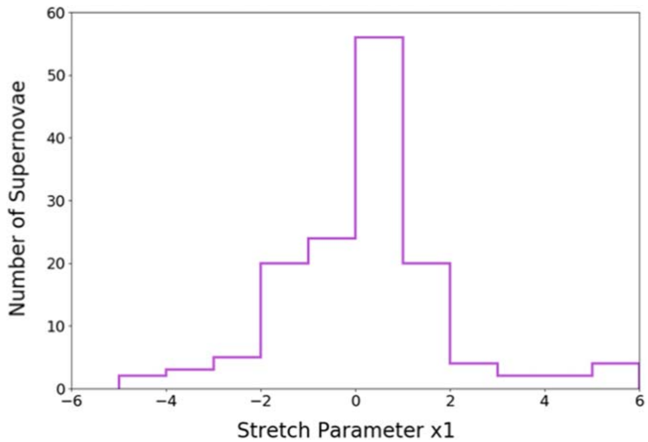

Figure 6. Distribution in the SALT stretch parameter x_1.

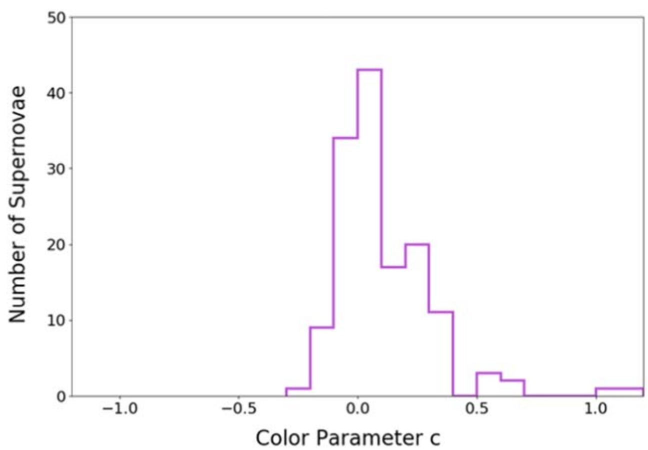

Figure 7. Distribution in the SALT color parameter c.

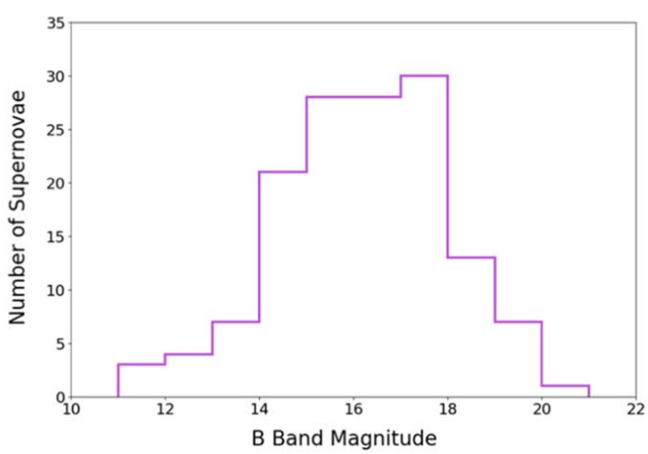

Figure 8. The distribution in $m_B{}^*$, the peak B band magnitude in the supernova rest frame, given by SALT.

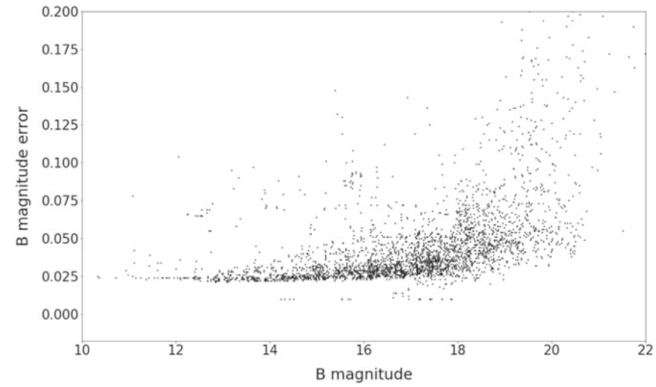

Figure 9. Scattergram of the B magnitude error vs. the B magnitude for individual measurements after calibration and galaxy background subtraction.

Table 6
Errors on LSQ13bug, B Filter, JD 2456529.53

Quantity	Value
Exposure Time	300 s
Instrumental Magnitude	20.216 ± 0.017
Instrumental Magnitude after Galaxy Subtraction	20.415 ± 0.026
Number of Field stars used for calibration	18
Zero point used for calibration	-2.664 ± 0.024
Calibrated Magnitude	17.751 ± 0.035

average zero-point for that observation was 0.024 mag, added in quadrature to the error on the subtracted magnitude to produce the 0.035 mag on the calibrated magnitude for this point on the light curve. It should be pointed out, however, that a systematic error or shift in the calibration of the APASS catalog will result in a similar systematic shift in the magnitudes of this sample.

The errors shown in Tables 4 and 6 are for one point on a light curve for one supernova. Figure 9 shows the scattergram of the error of all of the points on the lightcurves for each filter for this sample of supernovae versus their magnitude.

Many points on several filter light curves were used by SALT2.4 to estimate the rest frame B band peak magnitude m_B listed on Table 5. There were typically many points on the B and V light curves near peak brightness, so the errors on m_B were smaller than the errors on individual light curve points.

7. Conclusions

In this paper light curves for a sample of 140 low-redshift supernovae are presented in typically 5 filters: B, V, g, r, and i. The first few lines of these light curves are shown in Table 4. The whole set of light curves are available in electronic form. The procedures used in obtaining these light curves are described and the errors on the magnitudes in the light curves are discussed.

This research was supported at Yale by DOE grant DE FG0 ER92 40704 and The Yale University Provosts Office. We thank Dr. Andreas Kaufer, ESO, and the staff of the LaSilla Observatory for their cooperation in making the La Silla-QUEST project possible. This work is based (in part) on observations collected at the European Organization for Astronomical Research in the Southern Hemisphere, Chile, as part of PESSTO, (the Public ESO Spectroscopic Survey for Transient Objects) ESO program 188.D-3003, 191.D-0935, 197.D-1075. This work makes use of observations from the Las Cumbres Observatory network. D.A.H., G.H., and C.M. were supported by NSF grant AST-1616484. J.B., D.H., and C.P. are supported by NSF grant AST-1911225. I.A. is a CIFAR Azrieli Global Scholar in the Gravity and the Extreme Universe Program and acknowledges support from that program, from the European Research Council (ERC) under the European Union's Horizon 2020 research and innovation program (grant agreement No. 852097), from the Israel Science Foundation (grant Nos. 2108/18 and 2752/19), from the United States—Israel Binational Science Foundation (BSF), and from the Israeli Council for Higher Education Alon Fellowship. This research was made possible through the use of the AAVSO Photometric All-Sky Survey (APASS), funded by the Robert Martin Ayers Sciences Fund and NSF AST-1412587.

Appendix

This appendix lists a number of data tables that are too long to be included in the printed version of this article but are available as machine readable electronic tables.

Table A2
LCO 1 m Telescopes Filter Transmissions

nm	*B*	*V*	*g*	*r*	*i*
300	0.0000	0.0000	0.0000	0.0000	0.0000
301	0.0000	0.0000	0.0000	0.0000	0.0000
302	0.0000	0.0000	0.0000	0.0000	0.0000
303	0.0000	0.0000	0.0000	0.0000	0.0000
304	0.0000	0.0000	0.0000	0.0000	0.0000
305	0.0000	0.0000	0.0000	0.0000	0.0000
306	0.0000	0.0000	0.0000	0.0000	0.0000
307	0.0000	0.0000	0.0000	0.0000	0.0000
308	0.0000	0.0000	0.0000	0.0000	0.0000
309	0.0000	0.0000	0.0000	0.0000	0.0000
310	0.0000	0.0000	0.0000	0.0000	0.0000

(This table is available in its entirety in machine-readable form in the online version of this article.)

Table A3
Quantum Efficiencies of the SBIG and the Sinistro Cameras Used with the LCO 1 Meter Telescopes

Lambda (nm)	SBIG QE	Sinistro QE
300	0.003	0.66
350	0.233	0.75
400	0.415	0.92
450	0.442	0.92
500	0.546	0.91
550	0.598	0.93
600	0.556	0.91
650	0.483	0.90
700	0.415	0.89
750	0.353	0.84
800	0.311	0.78

(This table is available in its entirety in machine-readable form in the online version of this article.)

Table A1
Lightcurves of the 140 Supernovae in the Five Filter Bands The dates are Julian Dates in Addition to 2400000 *F* Stands for Filter Band

Supernova	*F*	Date	*B* mag	*B*mag erro
LSQ13bug	*B*	56526.22267	18.112	0.037
LSQ13bug	*B*	56526.22631	18.114	0.037
LSQ13bug	*B*	56529.02932	17.798	0.029
LSQ13bug	*B*	56529.03296	17.792	0.030
LSQ13bug	*B*	56530.07598	17.680	0.029
LSQ13bug	*B*	56532.10382	17.633	0.027
LSQ13bug	*B*	56532.10748	17.639	0.027
LSQ13bug	*B*	56534.14398	17.573	0.026
LSQ13bug	*B*	56534.14763	17.583	0.026
LSQ13bug	*B*	56536.10488	17.643	0.026
LSQ13bug	*B*	56536.10853	17.656	0.026

(This table is available in its entirety in machine-readable form in the online version of this article.)

Table A4
Magnitudes from the APASS Survey for Observed Field Stars

Name	R.A.	Decl.	*B*	Berr	*V*	Verr	*g*	gerr	*r*	rerr	*i*	ierr
	(deg)	(deg)	(mag)	(mag)	(mag)	(mag)	(mag)	(mag)	(mag)	(mag)	(mag)	(mag)
LSQ13bug-001	317.26841	−26.89386	14.173	0.026	13.366	0.044	13.732	0.009	13.052	0.046	12.866	0.083
LSQ13bug-002	317.29711	−26.90999	14.206	0.024	13.491	0.057	13.790	0.012	13.250	0.056	13.115	0.071
LSQ13bug-003	317.30752	−26.89644	14.508	0.006	13.571	0.047	13.991	0.008	13.229	0.044	12.974	0.078
LSQ13bug-004	317.26723	−26.85954	14.430	0.024	13.792	0.031	14.058	0.011	13.587	0.054	13.470	0.100
LSQ13bug-005	317.17892	−26.89882	14.759	0.023	14.062	0.056	14.365	0.018	13.851	0.054	13.742	0.073
LSQ13bug-006	317.21774	−26.97762	15.054	0.019	14.226	0.054	14.613	0.007	13.964	0.049	13.771	0.105
LSQ13bug-007	317.20722	−26.83100	15.038	0.028	14.274	0.032	14.604	0.015	14.054	0.052	13.916	0.099
LSQ13bug-008	317.29150	−26.95510	15.182	0.026	14.416	0.045	14.757	0.032	14.191	0.059	14.028	0.068
LSQ13bug-009	317.23581	−26.81714	15.085	0.030	14.458	0.044	14.725	0.010	14.261	0.055	14.129	0.101
LSQ13bug-010	317.21749	−26.83295	15.446	0.032	14.497	0.034	14.937	0.007	14.181	0.053	13.951	0.084
LSQ13bug-011	317.32689	−26.88614	15.301	0.041	14.595	0.047	14.900	0.005	14.356	0.047	14.219	0.069

Note. (https://www.aavso.org/apass). A name for each field star has been assigned based on the name of the supernova. See text for details of the magnitude system.

(This table is available in its entirety in machine-readable form in the online version of this article.)

Table A5
Instrumental Magnitudes Measured for Field Standards

MJD	*F*	*M*	Merr	Name
6525.565880	*r*	14.064	0.002	LSQ13bug-007
6525.565880	*r*	14.196	0.002	LSQ13bug-008
6525.565880	*r*	14.294	0.003	LSQ13bug-009
6525.565880	*r*	14.197	0.002	LSQ13bug-010
6525.565880	*r*	14.372	0.003	LSQ13bug-011
6525.565880	*r*	17.075	0.023	LSQ13bug-012
6525.565880	*r*	14.396	0.003	LSQ13bug-013
6525.565880	*r*	15.131	0.004	LSQ13bug-014
6525.565880	*r*	15.300	0.005	LSQ13bug-015
6525.565880	*r*	15.352	0.005	LSQ13bug-016
6525.565880	*r*	15.287	0.005	LSQ13bug-017

Note. Each line lists the Modified Julian Date (MJD), the filter name (*F*), the magnitude (*M*), the magnitude uncertainty (Merr) and the name of the field star (this refers to the table of APASS magnitudes tabulated in the Appendix). Note that the magnitudes are in the natural system LCOGT. They are determined using the same zero-points as the supernova light-curve magnitudes tabulated in the paper.

(This table is available in its entirety in machine-readable form in the online version of this article.)

ORCID iDs

C. Baltay https://orcid.org/0000-0003-0424-8719
L. Grossman https://orcid.org/0000-0002-5464-2768
R. Howard https://orcid.org/0000-0002-9759-2094
I. Arcavi https://orcid.org/0000-0001-7090-4898
C. Contreras https://orcid.org/0000-0001-6293-9062
D. Hiramatsu https://orcid.org/0000-0002-1125-9187
G. Hossenzadeh https://orcid.org/0000-0002-0832-2974
C. Pellegrino https://orcid.org/0000-0002-9472-1279

References

Aldering, G., Adam, G., Antilogus, P., et al. 2002, Proc. SPIE, 61, 4863
Baltay, C., Rabinowitz, D., Andrews, P., et al. 2007, PASP, 119, 1287
Baltay, C., Rabinowitz, D., Hadjiyska, E., et al. 2013, PASP, 125, 683
Becker, A. A., Whitman, D. M., Boeshar, P. C., et al. 2004, ApJ, 611, 418
Bertin, E., & Arnouts, S. 1996, A&AS, 117, 393
Betoule, M., Kessler, R., Guy, J., et al. 2014, A&A, 568, A22
Brown, A. G. A., Vallenari, A., Prusti, T., et al. 2018, A&A, 616, A1
Brown, T. M., Balliber, N., Bianco, F. B., et al. 2013, PASP, 125, 1031
Chambers, K. C., Magnier, E. A., Metcalfe, N., et al. 2016, arXiv:1612.05560v4
Contreras, C., Hamuy, M., Phillips, M. M., et al. 2010, ApJ, 139, 519
Dekany, R., Smith, R., Riddle, R., et al. 2020, PASP, 132, 038001
Drake, A. J., Djorgovski, A. G., Mahabal, A., et al. 2009, ApJ, 696, 870
Guy, J., Astier, P., Baumont, S., et al. 2007, A&A, 466, 11
Guy, J., Sullivan, M., Conley, A., et al. 2010, A&A, 523, A7
Hamuy, M., Folatelli, G., Morelli, N., et al. 2006, PASP, 118, 2
Henden, A. A., Levine, S. E., Terrell, D., et al. 2012, AAVSO, 40, 430
Henden, A. A., Levine, S. E., Terrell, D., et al. 2018, AAS Meeting, 232, 223.06
Holoien, T. W. S., Stanek, K. Z., Kochanek, C. S., et al. 2017, MNRAS, 464, 2672
Hosseinzadeh, G., Sand, D. J., Valenti, S., et al. 2017, ApJL, 845, L11
Howell, D. A., Arcavi, I., Hosseinzadeh, G., et al. 2015, AAS Meeting, 225, 140.07
Landolt, A. U. 2009, AJ, 137, 4186
Law, N. M., Kulkarni, S. R., Dekany, R. G., et al. 2008, PASP, 121, 1395L
Lipumov, V. M., Kornilov, V., Gorbovskoy, E., et al. 2010, AdAst, 2010, 30L
Maguire, K., Sullivan, M., Pan, Y. C., et al. 2014, MNRAS, 444, 325M
Olling, R., Mushotsky, R., Shaya, E. J., et al. 2015, Natur, 521, 332
Phillips, M. M., Contreras, C., Hsiao, E. H., et al. 2019, PASP, 131, 014001H
Quiang, L., Wei, P., Shang, Z. H., et al. 2018, RAA, 18, 005
Rest, A., Scolnic, D., Foley, R., et al. 2014, ApJ, 795, 44
Schlafly, E. F., Finkbeiner, D. P., et al. 2011, ApJ, 737, 103
Schlegel, D., Finkbeiner, D. P., Dvis, M., et al. 1998, ApJ, 500, 525
Scolnic, D. M., Jones, D. O., Rest, A., et al. 2018, ApJ, 859, 101
Smartt, S. J., Valenti, S., Fraser, M., et al. 2015, A&A, 579, A40
Smith, J. A., Tucker, D. L., Kent, S., et al. 2002, AJ, 123, 2121
Tonry, J., Denneau, L., Heinze, A. N., et al. 2018, PASP, 130, 988
Udalsky, A., Kubiak, M., Szymanski, M., et al. 1997, AcA, 47, 319
Valenti, S., Howell, D. A., Stritzinger, M. D., et al. 2016, MNRAS, 459, 3939
Walker, E. S., Baltay, C., Campillary, A., et al. 2015, ApJS, 219, 13
Yaron, O., & Gal-Yam, A. 2012, PASP, 124, 688
Zhang, J. C., Wang, X. F., Mo, J., et al. 2020, PASP, 132, 125001
Zhang, T., Wang, X., Chen, J., et al. 2014, RAA, 15, 215